

Intracardiac Phased-Array Imaging: Methods and Initial Clinical Experience With High Resolution, Under Blood Visualization

Initial Experience With Intracardiac Phased-Array Ultrasound

Douglas L. Packer, MD, Carolyn L. Stevens, RN, BSN, Michael G. Curley, PhD,
Charles J. Bruce, MD, Fletcher A. Miller, MD, Bijoy K. Khandheria, MD,
Jae K. Oh, MD, Lawrence J. Sinak, MD, James B. Seward, MD

Rochester, Minnesota

OBJECTIVES	This study was designed to test the feasibility of high-resolution phased-array intracardiac imaging.
BACKGROUND	Intracardiac echocardiographic imaging of the heart during interventional electrophysiologic (EP) procedures has been limited by inadequate ultrasound penetration and absence of Doppler hemodynamic and flow information produced by rotating mechanical ultrasound elements.
METHODS	A 10F (3.2 mm) phased-array, variable 5.5 to 10 MHz frequency imaging catheter with a four-way deflectable tip was applied in 24 patients undergoing EP studies. Sixteen prespecified cardiac targets were imaged from a right heart venue.
RESULTS	Fifteen patients had no underlying organic heart disease; nine had ischemic, cardiomyopathic, valvular or congenital heart disorders. Longitudinal and short-axis imaging readily disclosed each cardiac valve, support structures and chamber, as well as the pericardium, right and left atrial appendages, the junction of the right atrium and superior vena cava, crista terminalis, tricuspid valve isthmus, coronary sinus orifice, membranous fossa ovalis and pulmonary veins. The average target depth was 8.8 ± 1.5 cm (range 0.5 to 15 cm), with adequate penetration at a 7.5 MHz imaging frequency. Color flow and Doppler utilities clearly characterized transaortic and pulmonic valve and pulmonary vein blood flow, including during low output states.
CONCLUSIONS	These first human studies with this technology demonstrate the methods, feasibility and utility of intracardiac phased-array vector and Doppler imaging for long-axis, apex-to-base global cardiac imaging. High resolution of endocardial structures and catheters suggests additional utility for visualizing interventional procedures from the right heart. (J Am Coll Cardiol 2002;39:509-16) © 2002 by the American College of Cardiology

Over the past 20 years, interventional cardiac electrophysiology (EP) procedures have been performed almost exclusively under fluoroscopic guidance. Although this two-dimensional "silhouette" imaging provides a general representation of cardiac anatomy, it requires substantial experience to position an interventional device at a specific intracardiac target.

Transesophageal echocardiography has been employed in the catheterization lab as an alternative means of visualizing target endocardial, epicardial and valvular structures (1-8). Inherent limitations of this approach provided the incentive for developing single-operator, catheter-based echocardiographic techniques for more detailed anatomic imaging. Although single-element rotating mechanical systems have been applied to image right atrium (RA) anatomy for the

ablation of atrial tachycardias (9-13), limited penetration has been problematic.

Recently, catheter-based phased-array technology has been developed for obtaining deeper penetration, long- and short-axis images of intracardiac structures (14). Although this approach has been used in animals (14,15), it had not yet been tested in humans. This study was undertaken to test the feasibility of transcatheter, phased-array imaging for visualizing intracardiac structures and devices. Of paramount interest was the feasibility of left heart targeting from right heart chambers.

METHODS

This preclinical study followed a protocol approved by the Mayo Institutional Review Board. Twenty-four patients with cardiac arrhythmias initially underwent an EP evaluation. Fifteen had no other underlying heart disease while four had coronary artery disease, four had cardiomyopathies, one had congenital heart disease and one had valvular and ischemic heart disease.

From the Division of Cardiology, Mayo Foundation, Rochester, Minnesota. Sponsored by a grant from Acuson Corporation, Mountain View, California.

Manuscript received August 3, 2000; revised manuscript received October 10, 2001, accepted October 31, 2001.

Abbreviations and Acronyms

- EP = electrophysiologic, electrophysiology
- IVC = inferior vena cava
- LA = left atrium
- LV = left ventricle
- RA = right atrium
- RV = right ventricle
- SVC = superior vena cava

Ultrasound catheterization. Ultrasound imaging was undertaken after completion of the diagnostic or therapeutic procedure. One EP catheter was exchanged for an 11F hemostatic sheath, through which a 10F, 64-element, phased-array ultrasound imaging catheter was introduced. The catheter, with four-directional tip deflectability, was introduced into the RA. The catheter was coupled to a Sequoia ultrasound imaging platform (Acuson, Mountain View, California). Imaging frequency was optimized by the EP operator (D. L. P.) using adjunctive gain, depth and focal length controls. The imaging system also processed spectral color flow, pulsed wave, continuous wave and tissue Doppler images. Heparin anticoagulation, guided by the requirements of the EP study, ranged between 0 and 10,000 U.

Target imaging. Sixteen protocol-specific right and left heart structures were imaged solely from the RA or right ventricle (RV) at 5.5, 7.5, 8.5 and 10 MHz. These targets included the: 1) superior vena cava (SVC)/RA junction; 2) crista terminalis; 3) cavo-tricuspid isthmus; 4) coronary sinus orifice; 5) fossa ovalis; 6) low medial interatrial septum overlying the atrioventricular node; 7) tricuspid valve; 8) RV outflow tract; 9) left atrium (LA); 10) LA appendage; 11) orifice of all pulmonary veins; 12) mitral valve; 13) papillary muscles; 14) aortic and pulmonic valve leaflets; 15) systolic and diastolic left ventricle (LV) and RV endocardium; and 16) parietal pericardium. Intracardiac physiology in the region of valves, pulmonary veins and the interatrial septum

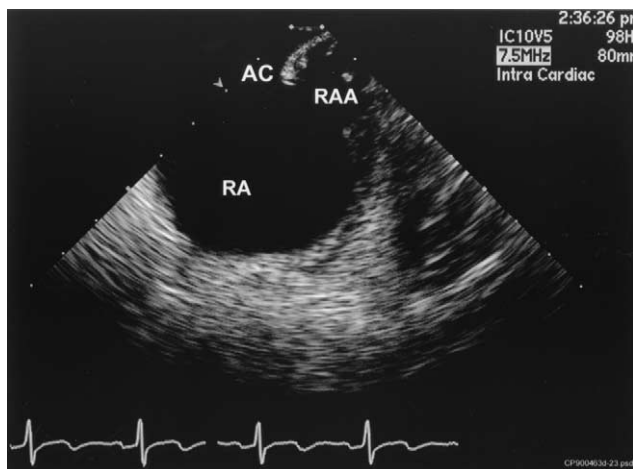


Figure 1. Right atrium (RA) at the superior vena cava/right atrial junction. Note the anterior crista (AC) ridge and trabeculae within the right atrial appendage (RAA). 1 cm calibration markers are also shown.

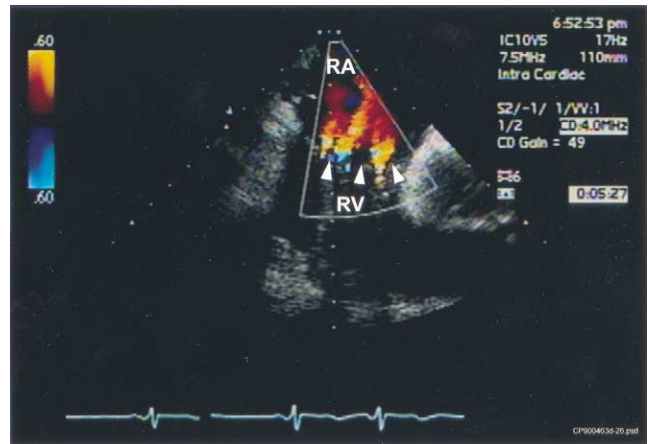


Figure 2. Color flow imaging demonstrating mild tricuspid valve insufficiency. Tricuspid insufficiency is noted as three jets of mid-range velocity (arrowheads) directed toward the imaging head. RA = right atrium; RV = right ventricle.

was examined with color flow and spectral Doppler. Any EP catheters used were targeted for visualization.

Statistical analysis. Digital clip images at the optimal imaging frequency were reviewed independently in a blinded manner by four reviewers (F. A. M., B. K. K., J. K. O., L. I. S.) skilled in the art of transesophageal echocardiography, with no financial relationship with the catheter/ultrasound system manufacturer. The optimized images were independently graded on a 0 to 5 scale for detail resolution, contrast resolution and uniformity: 0 = inability to image the target, 1 = poor image, 2 = fair, 3 = good, 4 = outstanding and 5 = exceptional image quality at that site. Correlation methods were used to assess the relationship between target depth and image score.

RESULTS

In each patient, the catheter was advanced via the right femoral vein into the RA. With experience, the catheter

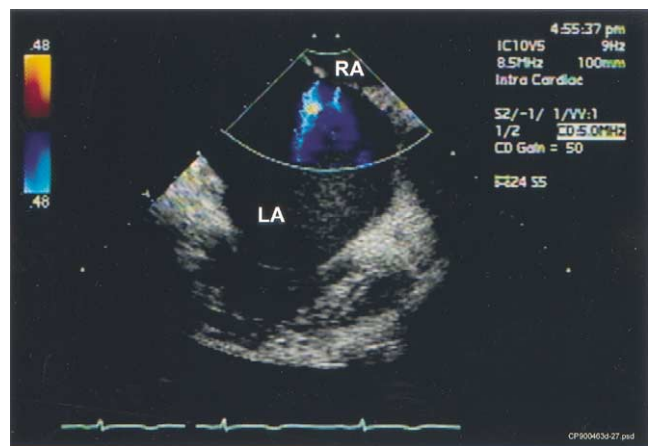


Figure 3. Membranous fossa ovalis obtained at an 8.5 MHz frequency from the right atrium (RA). The color flow image shows two jets directed into the left atrium (LA) across a fenestrated atrial septal defect.

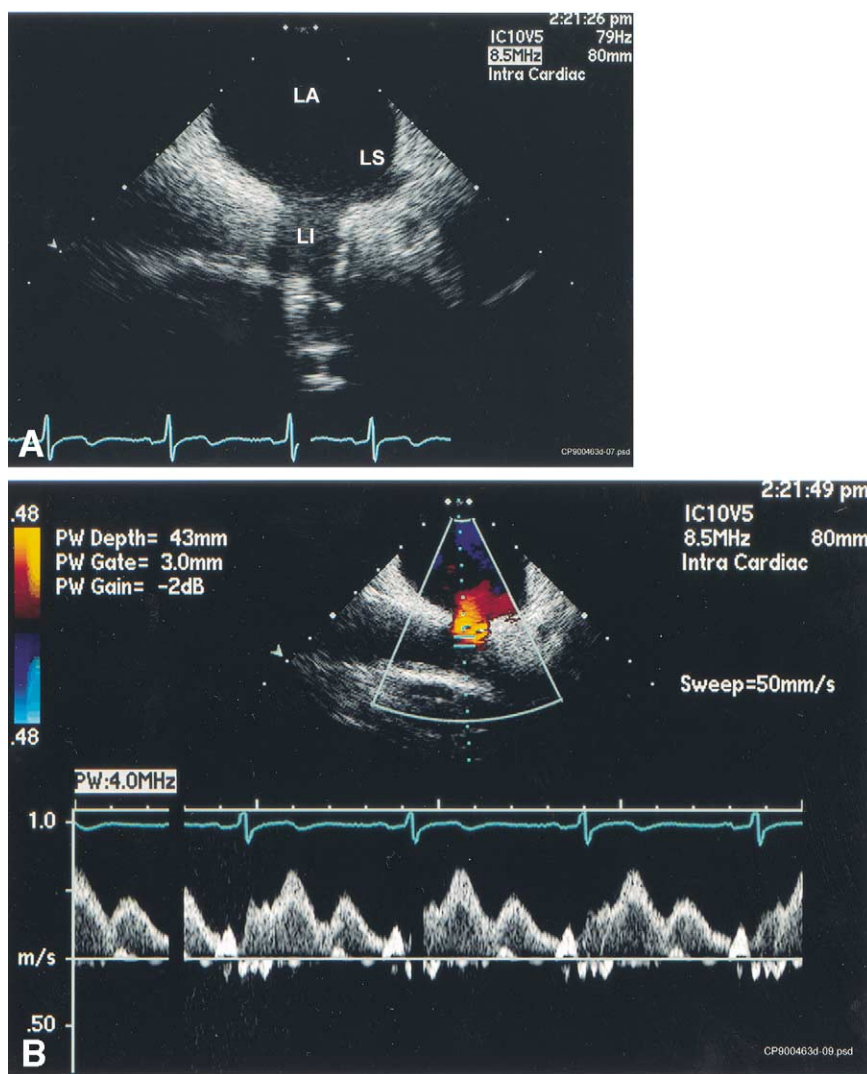


Figure 4. Left inferior (LI) and superior (LS) pulmonary veins entering into the posterior left atrium (LA). (A) The inferior vein entering from below and immediately to the left of the superior vein. (B) A pulsed wave Doppler tracing obtained from the inferior vessel.

could be advanced using tip deflectability without fluoroscopic guidance.

Right atrial targets. All RA targets were visualized by advancing or withdrawing the catheter to an appropriate level and rotating the catheter to bring the target into view. Tip-to-target distance ranged from 0.5 to 4.5 cm. Visualization of the anterior crista (Fig. 1) at the junction of the SVC and RA was enabled by positioning the imaging head, without tip deflection, in an anterior direction. Backward deflection of the catheter tip moved the image further from the imaging head whereas forward deflection of the tip moved the target closer. The best resolution of near- and mid-field structures was obtained at an 8.5 MHz frequency.

The tricuspid valve was best imaged by 10° to 30° anterior catheter tip deflection, beginning with the catheter in the mid-region of the RA. The presence of trivial to moderate tricuspid insufficiency was observed in 21 of 24 patients, as best demonstrated by 4.0 MHz Doppler color flow imaging (Fig. 2). Physiologic tricuspid insufficiency or back flow

related to the His bundle catheter was seen in 16 patients, whereas 5 had mild to moderate (grade 1 to 2/4) tricuspid regurgitation. Clockwise rotation of the catheter tip from an antero-lateral to antero-medial direction at the level of the inferior vena cava (IVC)/RA junction further visualized the isthmus of tissue between the tricuspid annulus and the IVC and the Eustachian ridge extending toward the coronary sinus orifice.

Interatrial septum. The interatrial septum was visualized in all patients by posteromedial (clockwise) rotation of a straight catheter tip positioned 0.5 to 2 cm above the IVC/RA junction. Posterior deflection of the imaging tip in the RA was occasionally required to optimize visualization of the fossa ovalis. The septum was intact in 22 patients but showed trivial trans-septal blood flow on color Doppler analysis in two patients: after trans-septal sheath removal in one patient and at the site of previous repair of an atrial septal defect in another. The multiple color flow jets characterizing a small right-to-left shunt are seen in

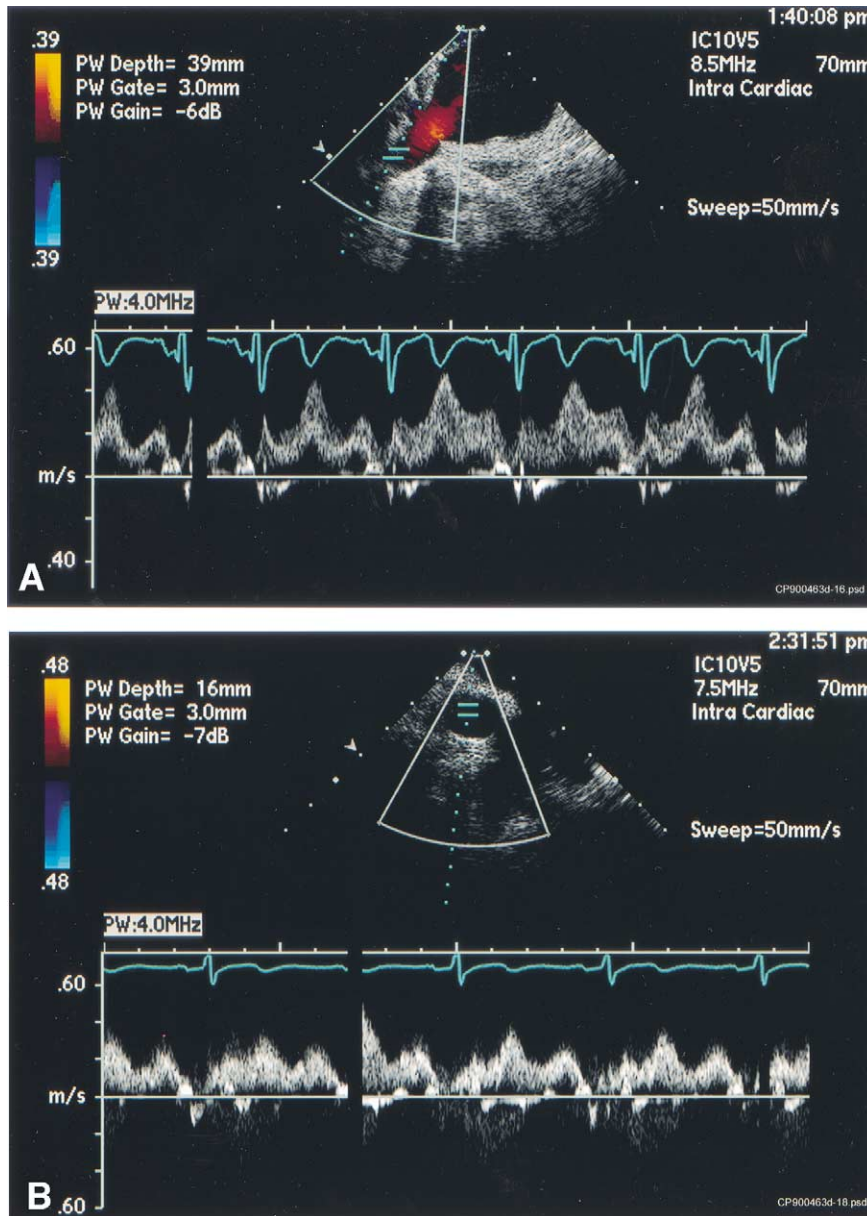


Figure 5. (A) Color flow and spectral Doppler imaging of the right inferior pulmonary vein. (B) Pulsed wave Doppler traces from the orifice of the right superior pulmonary vein. Here the vein orifice is viewed “en fas.”

Figure 3. An interatrial septal aneurysm was seen in three patients.

Left atrial structures. A 7.5 or 8.5 MHz imaging frequency optimized visualization of LA structures and pulmonary veins beyond the interatrial septum. Pulmonary vein imaging was uniformly possible by first visualizing the membranous fossa from a mid-to-low RA catheter tip position. With clockwise catheter rotation, the LA appendage could be visualized, followed by long-axis views of the left superior and inferior pulmonary veins. Figure 4A shows both left pulmonary veins entering into the postero-lateral aspect of the LA. Pulmonary vein inflow was consistently characterized under color flow and pulsed wave Doppler (Fig. 4B). Further clockwise rotation of the catheter brought the orifice of the right superior and inferior pulmonary veins

into view. The LA ostia of these veins were typically viewed “en fas,” yielding an “owl’s eyes” appearance at the vein’s orifice. Color flow and spectral pulsed wave Doppler flow patterns were as shown in Figure 5. With additional rotation, a long-axis view of the right superior pulmonary vein beyond its point of primary bifurcation was usually seen. **Great vessels.** Images of the LV and RV outflow tracts could be obtained from several locations. The optimal long-axis images were obtained with the catheter positioned at or slightly above the SVC/RA junction. With antero-medial to postero-medial (clockwise) catheter rotation and retraction, the entire length of the ascending aorta could be imaged. Short-axis or oblique views of the pulmonic valve were also obtainable from this position. Advancement of the catheter toward the innominate vein enabled aortic arch

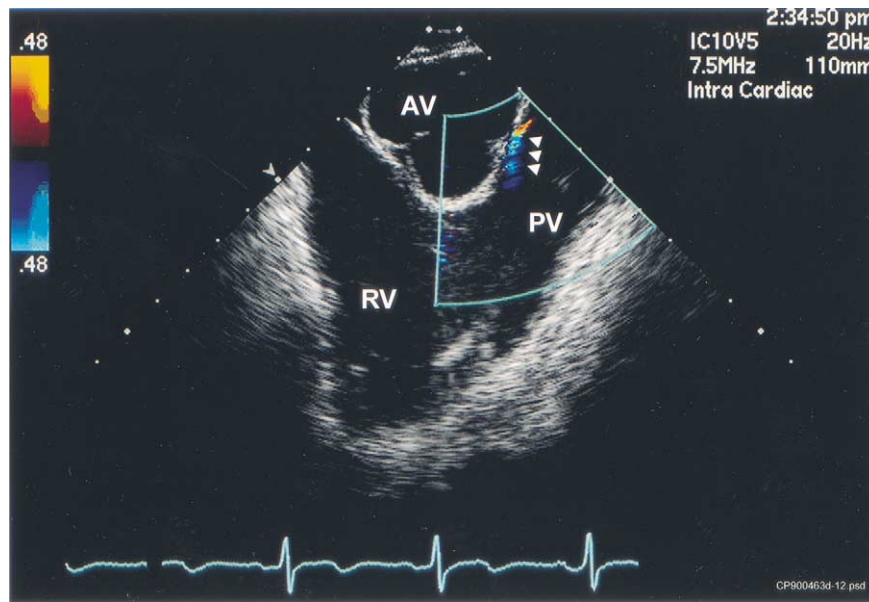


Figure 6. Cross-sectional view of the aortic valve (AV) leaflets seen from immediately above the tricuspid valve. The RV apex (RV), outflow tract and pulmonic valve (PV) are seen. Note the trivial pulmonic regurgitant jet (arrowheads).

visualization in every patient where attempted. Short-axis views of the LV outflow tract and aortic valve were best obtained from a point below the tricuspid valve with tip angulation toward the mid-RV outflow tract, or as visualized from above the valve as shown in Figure 6. Of the 21 patients with color flow Doppler imaging, 8 had no aortic valve insufficiency, 12 had trivial regurgitation and 1 had mild regurgitation.

Left ventricle targets. Imaging of each targeted LV structure at depths of 6 to 15 cm was accomplished with the catheter tip in a low RA position. Left ventricle long-axis imaging was best obtained by 30° anterior catheter tip deflection across the tricuspid valve near the septal commissure, with a 1 to 2 cm catheter extension into the base of the RV outflow tract (Fig. 7). A short-axis view of the LV, as well as the mitral valve (Fig. 8), was obtainable from the lateral base of the RV outflow tract after catheter straightening. Further clockwise rotation and occasional catheter back deflection were required to shift from an oblique to a short-axis image. Upon spectral Doppler imaging in 21 patients, 13 had trivial and 8 had no mitral insufficiency. Deflection and advancement of the catheter tip into the RV cavity was accomplished without interrupting the imaging process and without fluoroscopic guidance.

Visualization of indwelling catheters. Long-axis images of intracardiac EP catheters were obtained by initially identifying the entrance of the catheter shaft from the IVC into the RA. Because the catheters typically run with the long axis of the heart, minimal ultrasound catheter rotation was required to follow the catheter from this entrance site to the catheter tip/endocardial interface (Fig. 9).

Left heart image adequacy. The depth of targets is averaged in Table 1. The closest imaging depth was seen with visualization of the SVC/RA junction (0.5 cm). In

contrast, the greatest target distance was typically seen with LV apex imaging at 8.3 ± 0.5 cm (range to 15 cm). The mean maximal penetration seen with right heart imaging was 11.4 ± 1.1 cm. The time required to move from one target to another ranged from 5 to 20 s. The total procedural time to obtain all 16 targets at four imaging frequencies, along with all Doppler studies, ranged between 30 and 40 min. In the first 10 patients, 2.7 ± 2.2 min of fluoroscopy time was used to guide ultrasound catheter placement; this decreased to 1.7 ± 1.1 min in the last 10 patients.

Average target resolution, as determined by independent reviewers, was as seen in Table 1. The average detail resolution score ranged from 3.9 to 4.6 (4.3 ± 0.2) for RA structures, 3.7 to 4.7 (4.2 ± 0.2) for RV structures, 3.2 to 4.2 (3.7 ± 0.3) for LA structures, and from 3.6 to 4.2 (4.0 ± 0.4) for LV structures. The relationship between target resolution and depth showed a limited slope. In general, the 7.5 to 8.5 MHz imaging frequency was adequate for complete LV visualization. No major complications were encountered in this study.

DISCUSSION

This pilot human experience, with a high-resolution phased-array under blood imaging catheter, demonstrates the feasibility of long-axis visualization of right- and left-sided cardiac structures from the right heart. Depth of field extended from 0.5 cm in front of the lens to depths of 10 to 15 cm. This phased-array technology permitted a full gamut of imaging projections, including off-axis and short-axis visualization. The addition of Doppler imaging enhanced the ease of target assessment and showed potential for examining intracardiac hemodynamics and physiology.

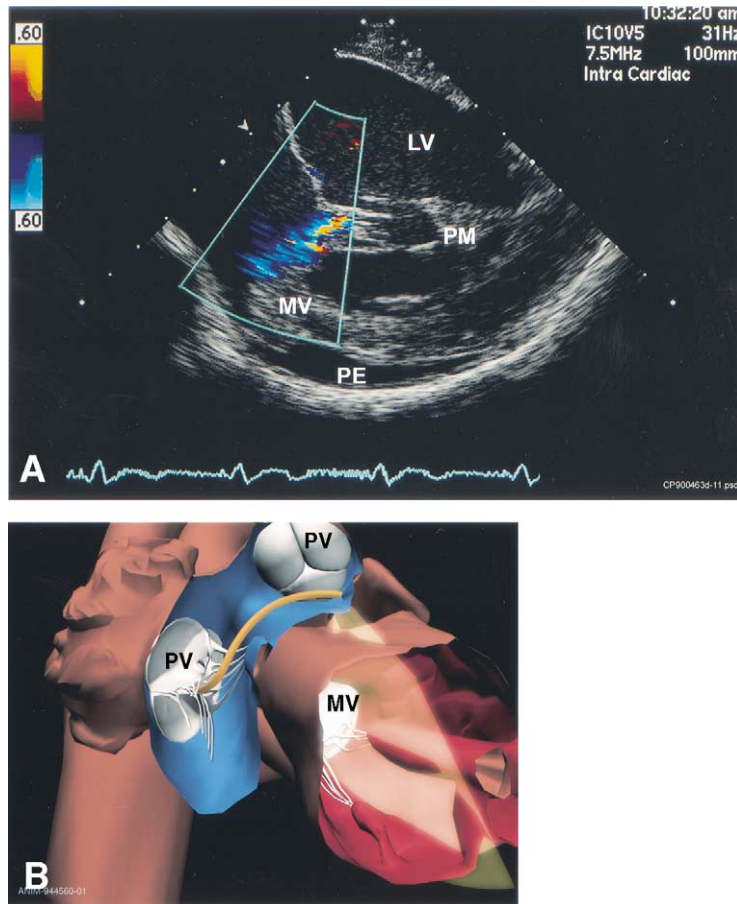


Figure 7. (A) Long-axis view of the left ventricle (LV) obtained from within the right ventricular outflow tract. Note the mitral valve (MV), chamber dilation, papillary muscles (PM) and an eccentric jet of mild mitral insufficiency. Also present is a small loculated posterior pericardial effusion (PE). (B) Catheter positioned across the tricuspid valve (TV) into the outflow tract used to obtain Figures 7 and 8. PV = pulmonic valve.

Mechanical/rotational imaging. Previous human applications of intracardiac ultrasound have been limited to those generated by the mechanical rotation of a single piezoelectric element in 6F to 10F catheters. Miniaturization of these elements required the use of higher 10 to 20 MHz trans-

ducer frequencies, limiting ultrasound penetration to surrounding cardiac tissues. This technology has been applied for the imaging of RA structures in humans (9-13,16,17) and animals (18-21), the membranous fossa ovalis (22,23), the crista terminalis (13), Eustachian ridge (9,10), tricuspid

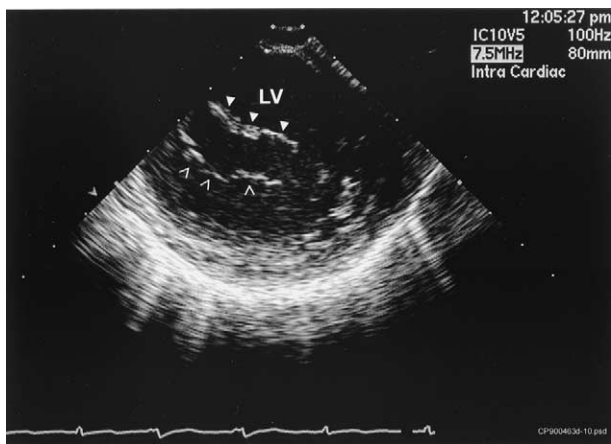


Figure 8. Short-axis left ventricular (LV) view at the level of the anterior (arrowheads) and posterior (open arrowheads) mitral valve leaflets. This image is obtained across the intraventricular septum with the catheter tip positioned in the right ventricular outflow tract.

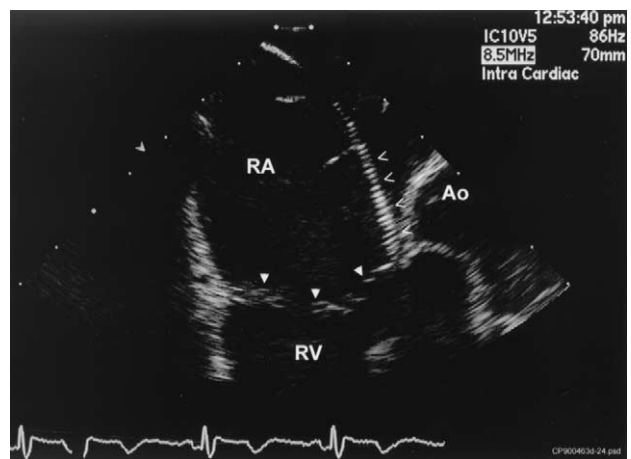


Figure 9. Multipolar His bundle recording electrode catheter is seen coursing from the right atrium (RA) to the medial aspect of the tricuspid valve (arrowheads). Ao = aortic root; RV = right ventricle.

Table 1. Image Depth and Scoring

	Target Depth (cm)	Detail Resolution	Contrast Resolution	Uniformity	Total Image Depth (cm)
Crista terminals	2.7 ± 0.7	4.1 ± 0.1	4.2 ± 0.1	4.2 ± 0.1	6.5 ± 1.2
Isthmus	2.8 ± 0.4	4.4 ± 0.1	4.4 ± 0.2	4.5 ± 0.2	8.8 ± 1.0
Fossa ovalis	2.5 ± 0.5	4.6 ± 0.6	4.6 ± 0.2	4.7 ± 0.2	9.0 ± 0.9
Tricuspid valve	4.3 ± 0.7	4.7 ± 0.1	4.7 ± 0.1	4.8 ± 0.1	10.2 ± 1.1
RV outflow tract	6.7 ± 0.7	3.7 ± 0.2	3.9 ± 0.2	4.0 ± 0.2	11.4 ± 1.1
Left atrium	6.2 ± 0.6	4.2 ± 0.1	4.3 ± 0.1	4.3 ± 0.1	9.7 ± 0.8
Left atrial appendage	6.9 ± 0.6	3.2 ± 0.3	3.4 ± 0.2	3.5 ± 0.2	9.7 ± 1.1
Aortic valve	—	3.8 ± 0.5	4.0 ± 0.5	4.0 ± 0.4	10.3 ± 0.8
Mitral valve	4.8 ± 0.7	3.9 ± 0.2	4.2 ± 0.1	4.1 ± 0.1	10.1 ± 0.4
Papillary muscles (LV)	5.7 ± 0.5	3.6 ± 0.5	4.0 ± 0.4	4.0 ± 0.3	10.2 ± 0.5
LV	8.3 ± 0.5	4.1 ± 0.4	4.2 ± 0.3	4.2 ± 0.2	10.1 ± 1.0
Pericardium	7.5 ± 1.2	4.2 ± 0.3	4.3 ± 0.2	4.4 ± 0.2	11.4 ± 1.1

LV = left ventricle; RV = right ventricle.

annulus (9,10) and the SVC/RA junction in the region of the sinoatrial node (11,18). These images have increased the understanding of the role of underlying anatomy in the pathophysiology of atrial arrhythmias and have aided the ablation of the posterior tricuspid isthmus in atrial flutter (9,10), or other RA tachycardias (12).

Such short-axis imaging produces high quality, high resolution near-field images, particularly suited for the assessment of coronary artery stenoses (24) and stent placement (25), as well as for other larger vessel imaging (26). Here, the cross-sectional “context” of an image is created by the near-field structures in front, as well as those to the left, right or behind the catheter tip. Because images are orthogonal to the orientation of cardiac chambers, catheters typically appear in their cross-section.

Longitudinal phased-array imaging. Previously, alternative phased-array imaging was limited to transesophageal echocardiography. Phased-array technologies enabled 5.5 to 7.5 MHz frequency examinations, allowing greater depth of penetration. Transesophageal imaging has been used to guide ablation of ventricular tachycardia (3) and accessory pathways (1,2,4), as well as trans-septal catheterization (7), and for the closure of atrial septal defects or cardiac biopsy (8,27). This approach has been limited in the interventional arena by aspiration risk and patient discomfort accompanying prolonged esophageal intubation and requires a second ultrasound operator to complete the study.

This study demonstrates the feasibility of deeper field, standard intracardiac visualization of specific right- and left-sided cardiac structures, as well as color flow and pulsed and continuous-wave Doppler imaging by a single operator. Intracardiac imaging from within a cardiac chamber presents several important “context” differences from transesophageal imaging. For example, LA structures are located laterally and posteriorly to the RA venue rather than anteriorly to those utilized in transesophageal imaging. Furthermore, the imaging catheter follows cardiac motion better with less target image motion than seen with transesophageal echocardiography.

Study limitations. LONGITUDINAL IMAGING PLANE. Images generated in this study were primarily in the long axis

of the catheter. Although a superior device might eventually have multiplane or three-dimensional visualization capabilities, the longitudinal imaging plane is in the major axis of the heart and most interventional devices. Furthermore, with catheter tip manipulation, short-axis images, as seen in Figure 9, are readily obtainable. As such, this is not likely to be a significant problem, compared to the limitations of other currently available alternative ultrasound devices.

DEVICE SIZE. The 10F catheter size required for housing the 64-element transducer is large and, therefore, initially recommended for venous side applications. Although this size is not unusual in the setting of current interventional practice, this limitation will be eliminated with the development of 7F and 8F catheters.

INTERVENTIONALIST UTILIZATION. The intent of interventional, intracardiac echocardiography is to allow the operator to perform user-specific, anatomic and hemodynamic examinations to assess underlying disease and guide therapy. The use of this technology will require the development of substantial ultrasound imaging skills, particularly given the nonstandard ultrasound images. The steepness of the learning curve will depend on the cumulative echocardiographic experience of a given user as required by a given intervention. Clearly, the evolving field of high resolution intracardiac imaging and physiologic visualization is in its infancy.

Clinical implications. The advantage of intracardiac imaging for diagnostic purposes is readily apparent. Single-operator use enhances the anatomic and physiologic understanding of the disease process. In the interventional EP arena, effective ablation of cardiac tissue is dependent, in part, on the extent of contact between the ablation catheter tip and the endocardial surface (28). This can be established in more than 95% of cases from an RA or RV imaging venue. Previous studies have documented the possibility of visualizing the evolving ablation lesion during 60% to 90% of radiofrequency energy deliveries (27). Even though the cost-effectiveness of these techniques will require additional clinical investigation, this study suggests a real-time means of guiding catheter placement and online assessment of the

results of specific interventions. This imaging approach may also lead to reductions in interventional fluoroscopic radiation exposures. Additional validation studies will be required to prove this benefit.

Reprint requests and correspondence: Dr. Douglas L. Packer, 4-416 Alfred Building, Mayo Foundation, Rochester, Minnesota 55905.

REFERENCES

- Packer D, Kapler J, Hammill S, Stanton M, Khandheria B, Seward J. Characterization of the pathophysiologic sequelae of the impedance rise during radiofrequency ablation of accessory pathways. *Circulation* 1991;84:II709.
- Goldman AP, Irwin JM, Glover MU, Mick W. Transesophageal echocardiography to improve positioning of radiofrequency ablation catheters in left-sided Wolff-Parkinson-White syndrome. *Pacing Clin Electrophysiol* 1991;14:1245–50.
- Saxon LA, Stevenson WG, Fonarow GC, et al. Transesophageal echocardiography during radiofrequency catheter ablation of ventricular tachycardia. *Am J Cardiol* 1993;72:658–61.
- Lai WW, al-Khatib Y, Klitzner TS, et al. Biplanar transesophageal echocardiographic direction of radiofrequency catheter ablation in children and adolescents with the Wolff-Parkinson-White syndrome. *Am J Cardiol* 1993;71:872–4.
- Drant SE, Klitzner TS, Shannon KM, Wetzel GT, Williams RG. Guidance of radiofrequency catheter ablation by transesophageal echocardiography in children with palliated single ventricle. *Am J Cardiol* 1995;76:1311–2.
- Ge S, Shiota T, Rice MJ, Hellenbrand WM, Sahn DJ. Images in cardiovascular medicine: Transesophageal ultrasound imaging during stent implantation to relieve superior vena cava to intra-atrial baffle obstruction after mustard repair of transposition of the great arteries. *Circulation* 1995;91:2679–80.
- Tucker KJ, Curtis AB, Murphy J, et al. Transesophageal echocardiographic guidance of transseptal left heart catheterization during radiofrequency ablation of left-sided accessory pathways in humans. *Pacing Clin Electrophysiol* 1996;19:272–81.
- Fehske W, Pfeiffer D, Babic U, Luderitz B. Images in cardiovascular medicine: Multiplane transesophageal imaging during transcatheter closure of an atrial septal defect. *Circulation* 1997;96:1702–3.
- Olgin JE, Kalman JM, Fitzpatrick AP, Lesh MD. Role of right atrial endocardial structures as barriers to conduction during human type I atrial flutter: Activation and entrainment mapping guided by intracardiac echocardiography. *Circulation* 1995;92:1839–48.
- Kalman JM, Olgin JE, Saxon LA, Fisher WG, Lee RJ, Lesh MD. Activation and entrainment mapping defines the tricuspid annulus as the anterior barrier in typical atrial flutter. *Circulation* 1996;94:398–406.
- Lee RJ, Kalman JM, Fitzpatrick AP, et al. Radiofrequency catheter modification of the sinus node for “inappropriate” sinus tachycardia. *Circulation* 1995;92:2919–28.
- Fisher WG, Pelini MA, Bacon ME. Adjunctive intracardiac echocardiography to guide slow pathway ablation in human atrioventricular nodal reentrant tachycardia: anatomic insights. *Circulation* 1997;96:3021–9.
- Kalman JM, Olgin JE, Karch MR, Hamdan M, Lee RJ, Lesh MD. “Cristal tachycardias”: origin of right atrial tachycardias from the crista terminalis identified by intracardiac echocardiography. *J Am Coll Cardiol* 1998;31:451–9.
- Seward JB, Packer DL, Chan RC, Curley M, Tajik AJ. Ultrasound cardioscopy: embarking on a new journey. *Mayo Clinic Proc* 1996;71:629–35.
- Packer D, Johnson S. Efficiency of ablation of atrial tissue with an irrigation tip catheter in the intact canine heart. *Pacing Clin Electrophysiol* 1996;19:651.
- Chu E, Kalman JM, Kwasman MA, et al. Intracardiac echocardiography during radiofrequency catheter ablation of cardiac arrhythmias in humans. *J Am Coll Cardiol* 1994;24:1351–7.
- Schwartz SL, Gillam LD, Weintraub AR, et al. Intracardiac echocardiography in humans using a small-sized (6F), low frequency (12.5 MHz) ultrasound catheter: Methods, imaging planes and clinical experience. *J Am Coll Cardiol* 1993;21:189–98.
- Kalman JLR, Fisher WG, Chin MC, et al. Radiofrequency catheter modification of sinus pacemaker function guided by intracardiac echocardiography. *Circulation* 1995:3070–81.
- Kalman JM, Jue J, Sudhir K, Fitzgerald P, Yock P, Lesh MD. In vitro quantification of radiofrequency ablation lesion size using intracardiac echocardiography in dogs. *Am J Cardiol* 1996;77:217–9.
- Olgin JE, Kalman JM, Chin M, et al. Electrophysiological effects of long, linear atrial lesions placed under intracardiac ultrasound guidance. *Circulation* 1997;96:2715–21.
- Ren JF, Schwartzman D, Michele JJ, et al. Intracardiac catheter echocardiographic (9MHz) imaging: in vivo validation and initial clinical applications (abstr). *J Am Soc Echocardiogr* 1997;10:406.
- Mitchel JF, Gillam LD, Sanzobrin BW, Hirst JA, McKay RG. Intracardiac ultrasound imaging during transseptal catheterization. *Chest* 1995;108:104–8.
- Epstein LM, Smith T, TenHoff H. Nonfluoroscopic trans-septal catheterization: safety and efficacy of intracardiac echocardiographic guidance. *J Cardiovasc Electrophysiol* 1998;9:625–30.
- Mintz GS, Painter JA, Pichard AD, et al. Atherosclerosis in angiographically “normal” coronary artery reference segments: an intravascular ultrasound study with clinical correlations. *J Am Coll Cardiol* 1995;25:1479–85.
- Mudra H, Klauss V, Blasini R. Ultrasound guidance of Palmaz-Schatz intracoronary stenting with a combined intravascular ultrasound balloon catheter. *Circulation* 1994;90:1252–61.
- Chavan A, Hausmann D, Dresler C, et al. Intravascular ultrasound-guided percutaneous fenestration of the intimal flap in the dissected aorta. *Circulation* 1997;96:2124–7.
- Segar DS, Bourdillon PD, Elsner G. Intracardiac echocardiography-guided biopsy of intracardiac masses. *J Am Soc Echocardiogr* 1995;6:927–9.
- Chugh S, Chan R, Johnson S, Packer DL. Catheter tip orientation affects radiofrequency ablation lesion size in the canine left ventricle. *Pacing Clin Electrophysiol* 1999;22:413–20.